Influence of oceanic ventilation and terrestrial transport on the atmospheric volatile chlorinated hydrocarbons over the Western Pacific

Shan-Shan Liu [a, b, 1], Jie Ni [a, 1], Jin- Ming Song[b], Xu-Xu Gao [a], Zhen He [a, c, *], Gui-Peng Yang [a, c, d, **]

[a] Frontiers Science Center for Deep Ocean Multispheres and Earth System, and Key Laboratory of Marine Chemistry Theory and Technology, Ministry of Education, Ocean University of China, Qingdao 266100, China

[b] Key Laboratory of Marine Ecology and Environmental Sciences, Institute of Oceanology, Chinese Academy of Sciences, Qingdao 266071, China

[c] Laboratory for Marine Ecology and Environmental Science, Qingdao Marine Science and Technology Center, Qingdao 266237, China

[d] Institute of Marine Chemistry, Ocean University of China, Qingdao 266100, China

---

[1] Shan-Shan Liu and Jie Ni contributed equally to the paper.

[*] Corresponding author. Key Laboratory of Marine Chemistry Theory and Technology, Ministry of Education, Ocean University of China, Qingdao 266100, China

[**] Corresponding author. Institute of Marine Chemistry, Ocean University of China, Qingdao 266100, China

E-mail addresses: zhenhe@ouc.edu.cn (Z. He), gpyang@mail.ouc.edu.cn (G.-P. Yang)

Contents of this file:

1. **Text S1**
2. **Figures: S1-S8**
3. **Table: S1**

1. Text S1 Oceanographic characteristics of the Western Pacific

As shown in Fig. 1B, the North Equatorial Current (NEC) in the central western Pacific is a broad easterly current located between 9°N and 18°N. It is characterized by high temperature, high salinity, high transparency, and low nutrient content. The NEC bifurcates off the coast of the Philippines into the poleward-flowing Kuroshio Current (KC) and the equatorward-flowing Mindanao Current. The KC continues eastward, becoming the Kuroshio Extension as it interacts with the low-salinity, high-nutrient waters of the Oyashio Current along Japan's east coast, forming the Kuroshio-Oyashio Extension (KOE). In the equatorial Pacific, the Equatorial Undercurrent flows swiftly eastward, creating a narrow band of saline, oxygen-rich water. As the region with the most precipitation, highest seawater temperature, and most active air-sea exchanges, the Western Pacific Warm Pool (WPWP) is crucial to the global climate system.

As shown in Fig. S1, sea surface temperature (SST) gradually increased from north to south, with the highest temperatures appearing near the equator. The North Pacific Subtropical Gyre (NPSG) area, dominated by the NEC, had a higher surface salinity than the WPWP. The WPWP strongly influences equatorial waters. These waters also receive heavy rainfall (up to 2 m annually), causing sharp decreases in surface salinity. The presence of high temperatures, high salinities, and low nutrient levels at depths of 50 to 250 m near the equator and between 12°N and 22°N were indicative of the influence of the Equatorial Undercurrent and the North Equatorial

Subsurface Current (Fig. S2). In higher-latitude seas, the Oyashio Current, carrying cold, fresh, nutrient-rich water, merges with the warm, saline, oligotrophic Kuroshio Intermediate Water, creating a distinct demarcation in subsurface temperature, salinity, dissolved oxygen, and nutrient levels.

2. Figures: S1-S8

Fig. S1. Horizontal distributions of temperature (a), salinity (b), Chl-*a* (c), $CHCl_3$ (d), CCl_4 (e), C_2HCl_3 (f), and CH_3CCl_3 (g) in surface seawater of the Western Pacific.

Fig. S2. Vertical profiles of temperature, salinity, Chl-*a*, and nutrients at depths of 0–200 m in the Western Pacific.

Fig. S3. 96 h back trajectories of air masses over the Western Pacific. The ensembled 96 h back-trajectories are within the lower troposphere above 10 m (red lines), above 100 m (blue lines), and above 1000 m (green lines).

Fig. S4. Linear correlations between the atmospheric mixing ratios of SF_6 and those of $CHCl_3$ (a) and C_2HCl_3 (b) in the Western Pacific.

Fig. S5. Linear correlations between the Chl-*a* concentration and atmospheric mixing ratios of $CHCl_3$ (a) and C_2HCl_3 (b) in the KOE area.

Fig. S6. (a) Interannual variations of wind speed (m/s) and SST (°C) in the study area and global interannual variability of CCl_4 in 2019. (b) Interannual variability of CCl_4 for 2019 in the GSN. (c) Interannual variability of CCl_4 from October 2020 to September 2021 in the SDZ. Wind speed data were sourced from the ERA5 dataset by Hersbach et al. (2020), and SST data were derived from ECCO2 cube92 dataset by Menemenlis et al. (2008). The CCl_4 data for the GSN were obtained from AGAGE network (https://agage.mit.edu/), and the CCl_4 data for the SDZ were derived from Yi et al. (2023).

Fig. S7. Relationship between the sea-air fluxes of CH_3CCl_3 (a) and CCl_4 (b) and wind speed and atmospheric concentrations of CH_3CCl_3 and CCl_4 (points are colored according to atmospheric concentrations).

Fig. S8. Relationship between the sea-air fluxes of CH_3CCl_3 (a) and CCl_4 (b) and

67 wind speed and SST (points are colored according to SST).

68

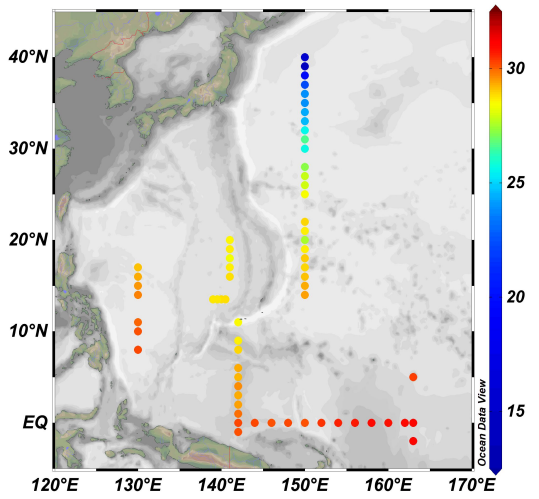

(a) Temperature (℃)

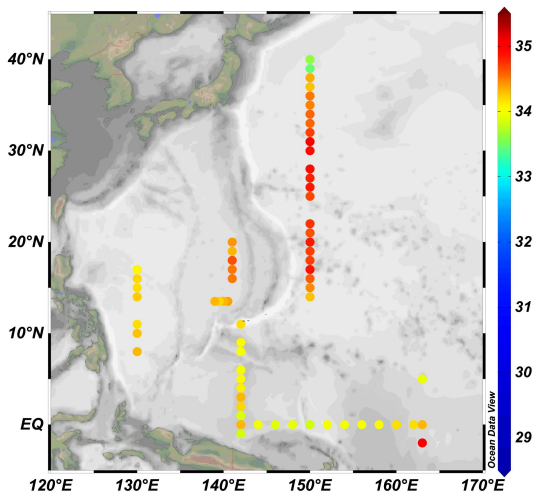

(b) Salinity

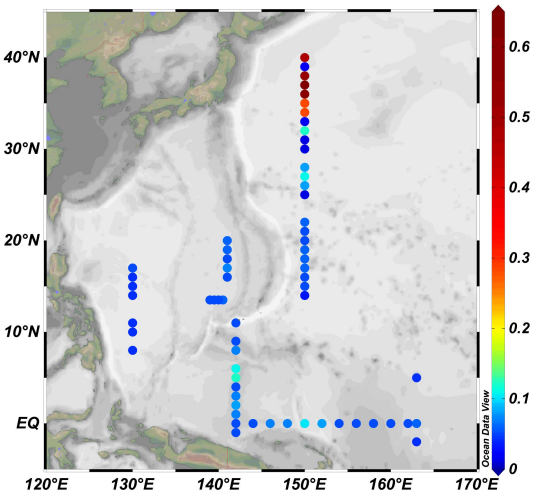

(c) Chl-*a* (μg·L^{-1})

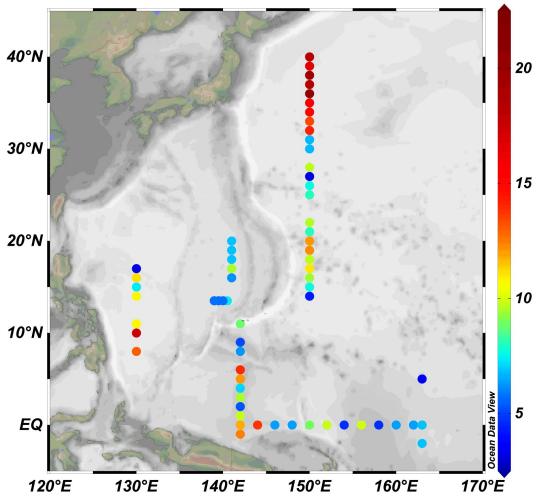

(d) $CHCl_3$ (pmol L^{-1})

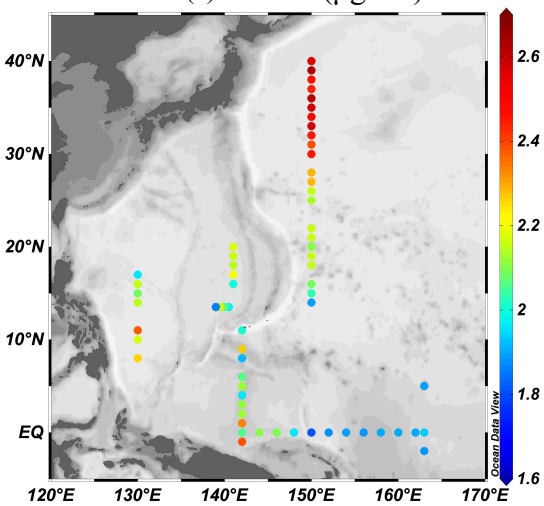

(e) CCl_4 (pmol L^{-1})

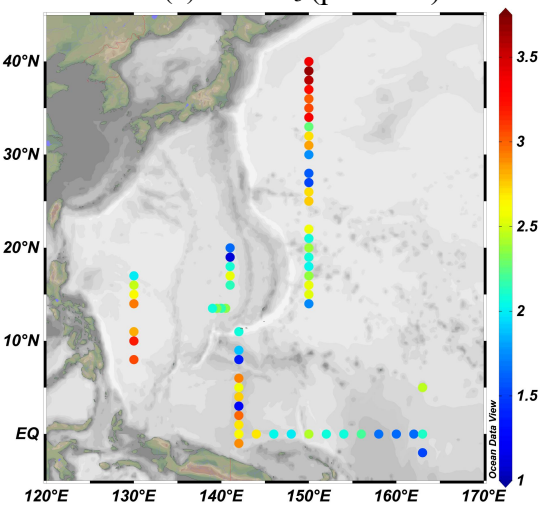

(f) C_2HCl_3 (pmol L^{-1})

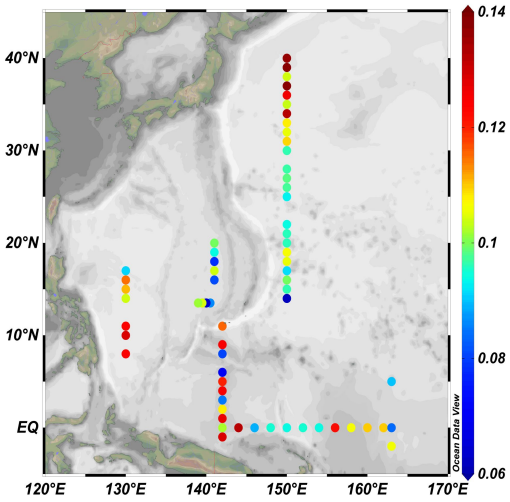

(g) CH_3CCl_3 (pmol L^{-1})

Fig. S1. Horizontal distributions of temperature (a), salinity (b), Chl-*a* (c), $CHCl_3$ (d), CCl_4 (e), C_2HCl_3 (f), and CH_3CCl_3 (g) in surface seawater of the Western Pacific.

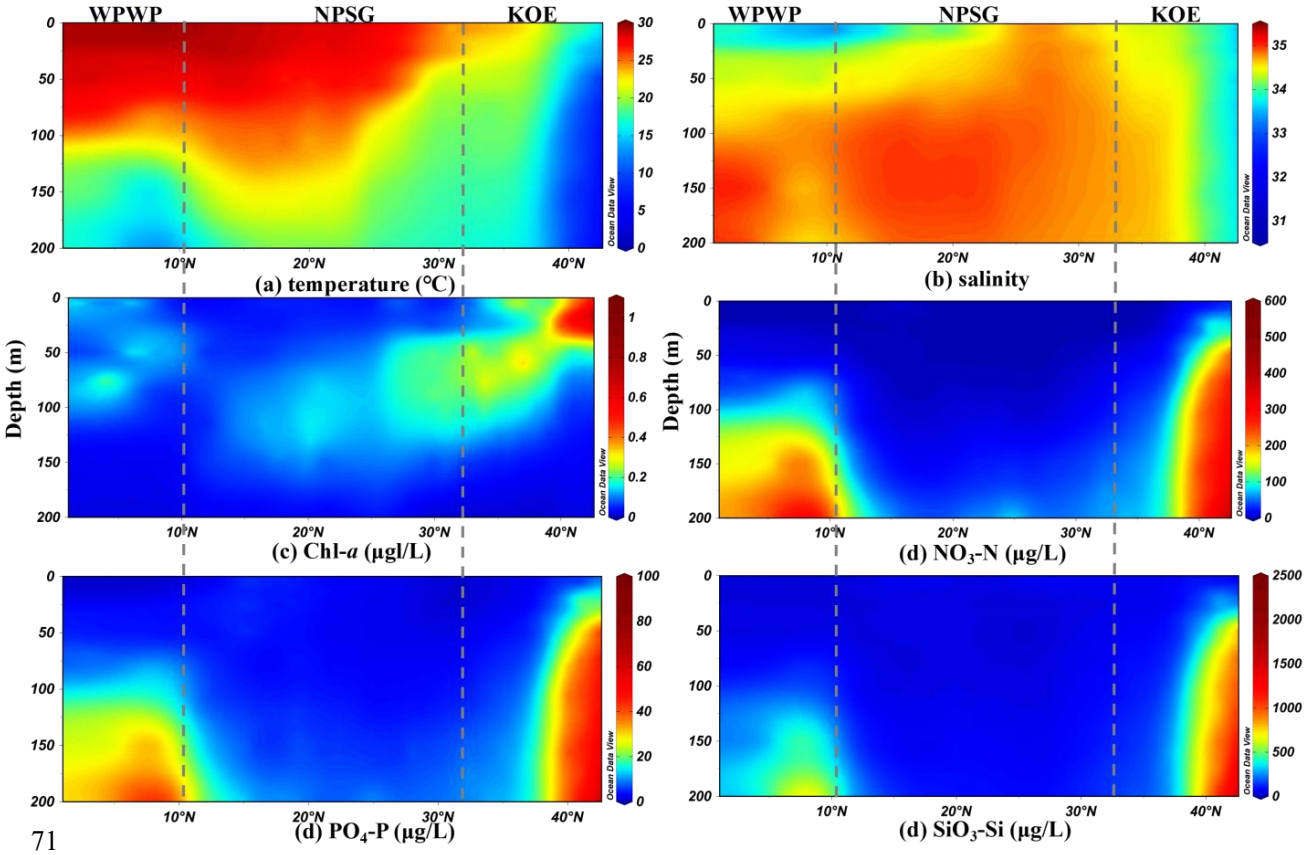

Fig. S2. Vertical profiles of temperature, salinity, Chl-*a*, and nutrients at depths of 0–200 m in the Western Pacific.

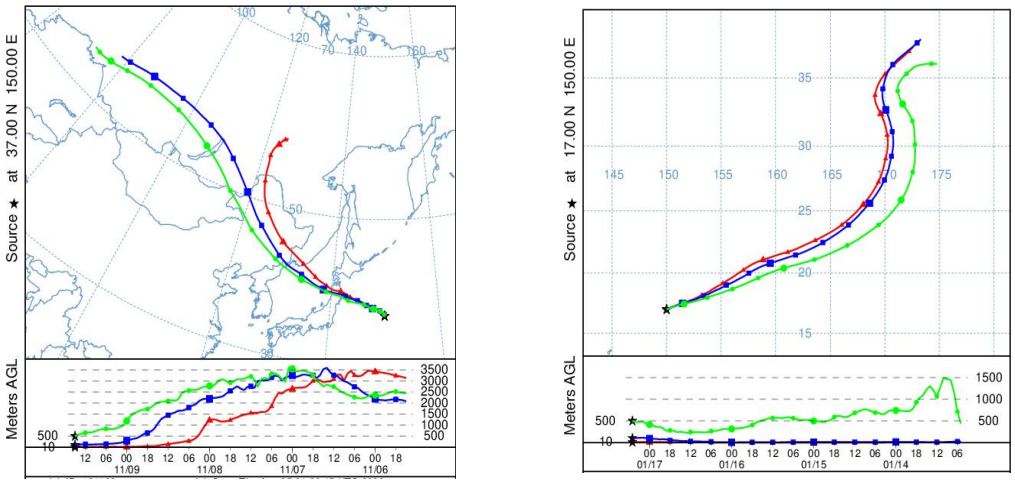

Station P1-4 Station P1-24

Fig. S3. 96 h back trajectories of air masses over the Western Pacific. The ensembled 96 h back-trajectories are within the lower troposphere above 10 m (red lines), above 100 m (blue lines), and above 1000 m (green lines).

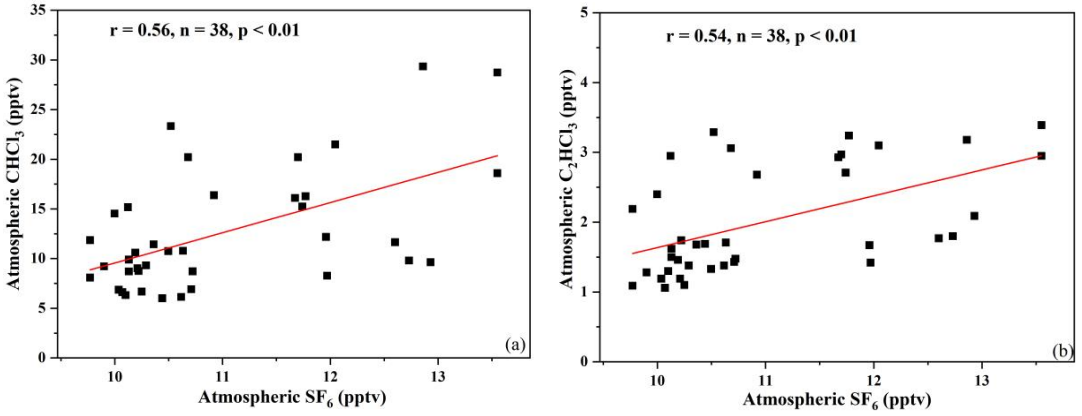

Fig. S4. Linear correlations between the atmospheric mixing ratios of SF_6 and those of $CHCl_3$ (a) and C_2HCl_3 (b) in the Western Pacific.

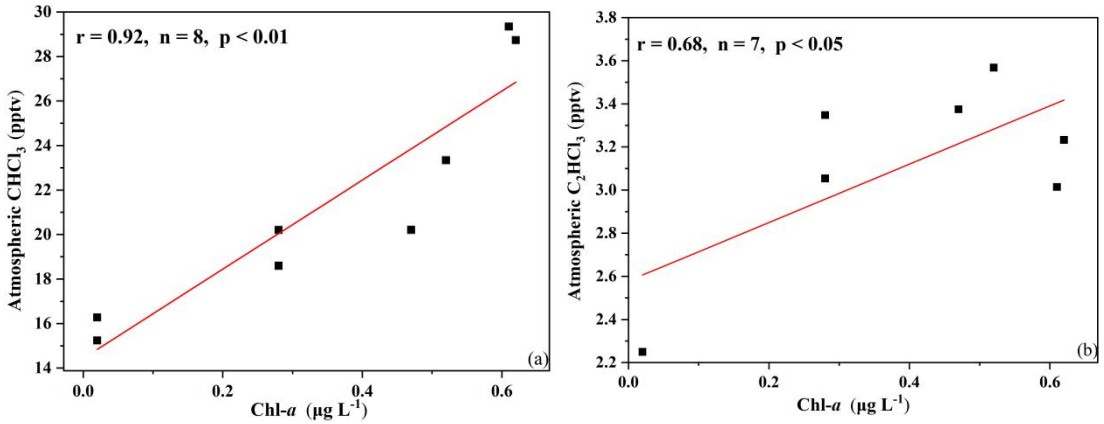

Fig. S5. Linear correlations between the Chl-*a* concentration and atmospheric mixing ratios of $CHCl_3$ (a) and C_2HCl_3 (b) in the KOE area.

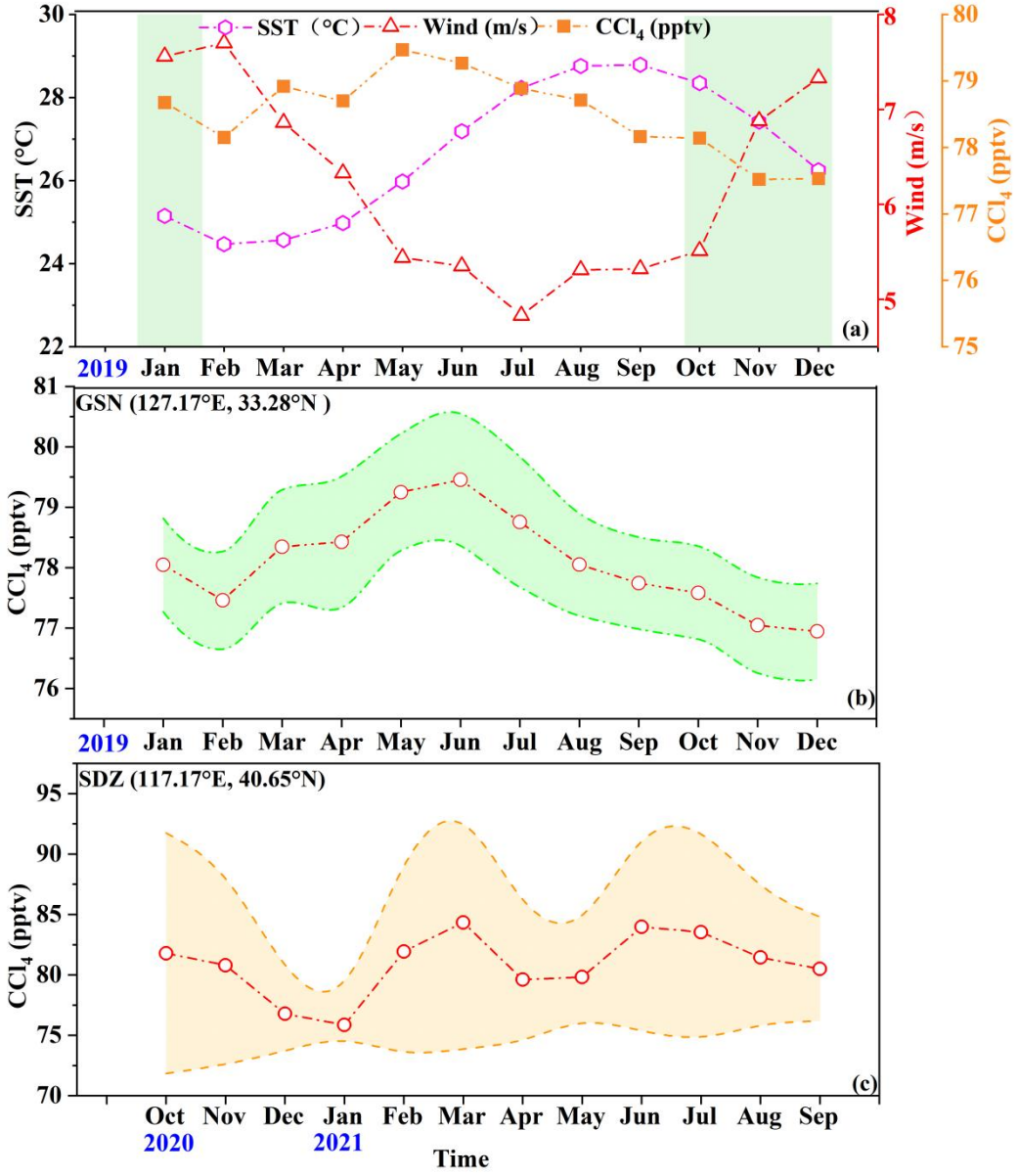

Fig. S6. (a) Interannual variations of wind speed (m/s) and SST (°C) in the study area and global interannual variability of CCl_4 in 2019. (b) Interannual variability of CCl_4 for 2019 in the GSN. (c) Interannual variability of CCl_4 from October 2020 to September 2021 in the SDZ. Wind speed data were sourced from the ERA5 dataset by Hersbach et al. (2020), and SST data were derived from ECCO2 cube92 dataset by

Menemenlis et al. (2008). The CCl_4 data for the GSN were obtained from AGAGE network (https://agage.mit.edu/), and the CCl_4 data for the SDZ were derived from Yi et al. (2023).

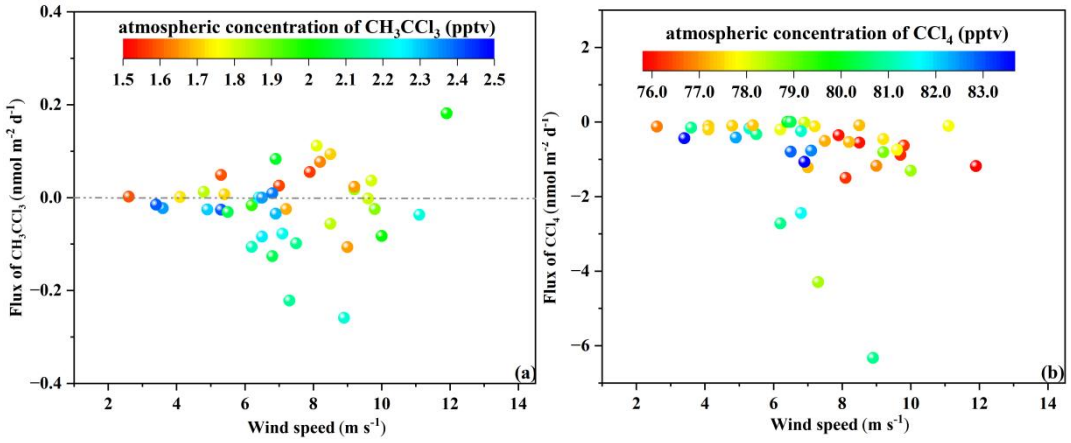

Fig. S7. Relationship between the sea-air fluxes of CH_3CCl_3 (a) and CCl_4 (b) and wind speed and atmospheric concentrations of CH_3CCl_3 and CCl_4 (points are colored according to atmospheric concentrations).

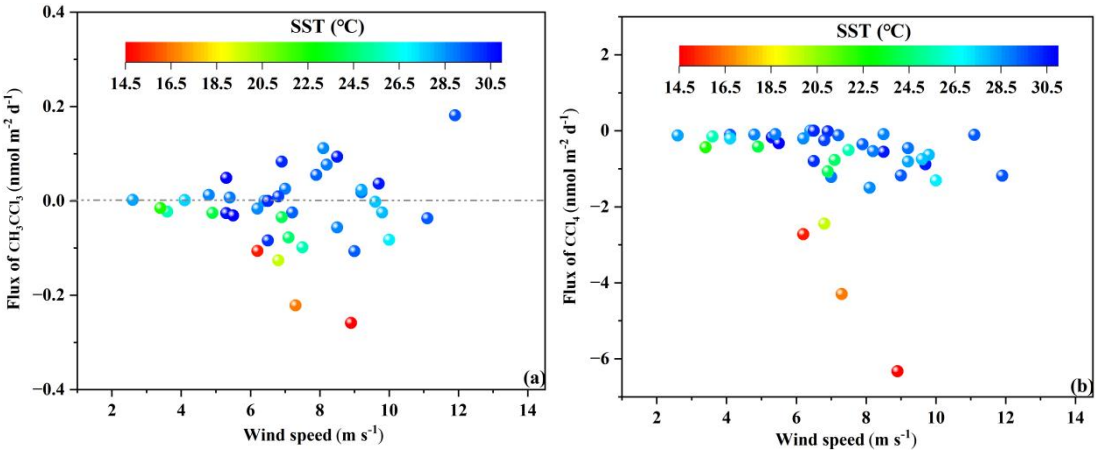

Fig. S8. Relationship between the sea-air fluxes of CH_3CCl_3 (a) and CCl_4 (b) and wind speed and SST (points are colored according to SST).

3. Table: S1

Table S1 Method detection limits (MDL), precision, and atmospheric lifetimes of the selected VCHCs.

Compound	Atmosphere (pptv)		Seawater (pmol L^{-1})		Lifetime [a]
	MDL	Precision (%)	MDL	Precision (%)	
$CHCl_3$	0.50	5	0.50	3	178 days
C_2HCl_3	0.10	3	0.20	9	5.6 days
CH_3CCl_3	0.20	6	0.05	5	5 years
CCl_4	1.00	4	0.10	7	30 years

[a] WMO (2022)